



HAL
open science

Two-exciton bound state quantum self-trapping in an extended star graph

Vincent Pouthier

► **To cite this version:**

Vincent Pouthier. Two-exciton bound state quantum self-trapping in an extended star graph. The Journal of Chemical Physics, 2022, 156 (15), pp.155101. 10.1063/5.0087200 . hal-03553414

HAL Id: hal-03553414

<https://hal.science/hal-03553414>

Submitted on 2 Feb 2022

HAL is a multi-disciplinary open access archive for the deposit and dissemination of scientific research documents, whether they are published or not. The documents may come from teaching and research institutions in France or abroad, or from public or private research centers.

L'archive ouverte pluridisciplinaire **HAL**, est destinée au dépôt et à la diffusion de documents scientifiques de niveau recherche, publiés ou non, émanant des établissements d'enseignement et de recherche français ou étrangers, des laboratoires publics ou privés.



Distributed under a Creative Commons Attribution 4.0 International License

Two-exciton bound state quantum self-trapping in an extended star graph.

Vincent Pouthier*

*Institut UTINAM, Université de Franche-Comté,
CNRS UMR 6213, 25030 Besançon Cedex, France*

(Dated: February 2, 2022)

The attractive Bose-Hubbard model is applied for describing the quantum self-trapping in an extended star graph. In the strong coupling limit and when two excitons are created on the core of the star, the dynamics is dominated by pair states whose properties is governed by the branch number N . When $N = 2$, the star reduces to a linear chain so that the energy does not self-localize. Conversely, when $N \geq 3$, a restructuring of the eigenstates arises and a low-energy state occurs describing a pair localized on the core of the star. Preferentially excited, this localized state gives rise to a quantum self-trapping of the energy, a process that intensifies as N increases.

PACS numbers:

I. INTRODUCTION

Exploiting the propagation of a quantum excitation in a complex network is a promising way for elaborating scalable quantum devices¹. For instance, in a dendrimer², electronic excitons play a central role to obtain an artificial light-harvesting complex³⁻⁹. To convert the energy of a radiation into a chemical fuel, the main idea consists in the functionalization of the terminal groups by chromophores that are responsible for light harvesting. The capture of light generates excitons that propagate towards the core that contains either a trap, a reaction center or a chemical sensor^{10,11}. Similarly, in complex networks, the exciton propagation defines a continuous time quantum walk (CTQW)¹² that is expected to be useful in quantum information processing¹³⁻¹⁹. It has been studied in a great variety of networks such as binary and glued trees²⁰, Apollonian networks²¹, fractal networks^{22,23}, sequentially growing networks²⁴ and star graphs²⁵⁻³¹.

In that context, to judge the efficiency of the excitonic propagation, the fundamental question arises whether the exciton propagates coherently or localizes along the network. Although the localization still remains an open problem, recent investigation suggests that the localized or delocalized nature of the exciton depends on general features such as its initial position, the presence of defects and the network topology¹.

Indeed, as shown by Mulken et al.³², localization processes may result from the degeneracy of the excitonic spectrum that originates in the symmetry of the network. In this case, when the excitonic state initially expands over few highly degenerate eigenstates, specific quantum self-interferences arise. The propagation of the exciton is thus stopped and the latter remains confined in the neighborhood of the excited region. As in solid-state physics, localization may also arise when the network is perturbed by defects. For instance, disordered site energies completely stop the quantum walk in linear chains³³, discrete rings³⁴, binary trees³⁵ and glued trees^{36,37}. Fi-

nally, the localization may originate in the architecture of the graph, as observed in extended dendrimers³⁸. In that case, exciton that propagates from the periphery to the core is prone to a localization-delocalization transition. This transition results from quantum interferences that arise due to the multiple scatterings that occur each time the exciton tunnels from one generation to another.

In this paper, a new facet of the localization in complex networks is addressed by investigating quantum self-trapping in nonlinear extended star graphs.

The concept of energy localization due to nonlinearity has been intensively studied in classical lattices with translational invariance³⁹⁻⁴¹. In that context, the discrete nonlinear Schrödinger (DNLS) equation plays a key role due to its relevance to interpret a large number of phenomena. This equation has revealed the occurrence of a remarkable feature known as the classical self-trapping mechanism⁴²: the local accumulation of energy remains trapped where it has been created. In the quantum regime, a different situation arises in lattices with translational invariance. The quantum equivalent of the DNLS equation is the Bose-Hubbard model⁴³⁻⁴⁵ in which the nonlinearity favors a coupling between bosonic excitations, called excitons in the following of the text. It leads to the occurrence of specific states, namely two-exciton bound states (TEBS)⁴⁵⁻⁵⁵, which have been observed in various molecular structures⁵⁶⁻⁶⁰. A TEBS corresponds to the trapping of two quanta over a few neighboring sites. The two excitons form a pair that behaves as a single particle delocalized along the lattice with a well-defined momentum. Although the pair cannot localize the energy, it takes a very long time to tunnel from one lattice site to another. Therefore, the initial excitation of two excitons on a single site produces a localization of the energy over a time scale that increases with the nonlinearity. This localized behavior, known as the quantum signature of the classical self-trapping, disappears in the long-time limit due to the nonvanishing dispersion of the bound-state energy band.

Beyond translational invariant lattices, TEBS were

studied very recently in a star graph⁶¹. In that case, it has been shown that when the excitons are created on the core of the star, the interplay between the architecture of the graph and the nonlinearity favors the occurrence of a real quantum self-trapping. Quite weak in the small nonlinearity limit, this self-localization is enhanced as the nonlinearity increases. This feature originates in the restructuring of the two-exciton eigenstates whose localized nature intensifies with the nonlinearity. Nevertheless, the quantum self-trapping is never complete since it is impossible to localize the entire exciton density.

In the present work, this previous study is generalized to the case of an extended star graph within the strong nonlinearity limit. In that case, owing to the extended nature of the branches of the star, it will be shown that the graph supports a TEBS that localizes exponentially on the core of the star. As a result, depending on the architecture of the network, a strong self-trapping can be obtained when two excitons are initially created on the core of the graph.

The paper is organized as follows. In Sec. II the extended star graph is introduced and the exciton Bose-Hubbard Hamiltonian is defined. Then the Schrodinger equation is established in the strong coupling. The problem is solved numerically in Sec. III and the results are finally discussed and interpreted in Sec. IV.

II. THEORETICAL BACKGROUND

A. Model Hamiltonian

As shown in Fig. 1, we consider the extended star graph formed by N branches that emanate out from a central node. Each branch B_ℓ , with $\ell = 1, \dots, N$, corresponds to a semi-infinite chain whose nodes are labeled by the index $s = 1, 2, 3, \dots$. The central node, denoted $(\ell = 0, s = 0)$, is connected to the side site $s = 1$ of each branch.

On this network, we are interested in the motion of bosonic excitations, called excitons, whose quantum dynamics is described according as the Bose version of the Hubbard model. Within this model, each site (ℓ, s) is occupied by a molecular subunit whose internal dynamics is described by an anharmonic oscillator. By denoting $b_{\ell s}^\dagger$ and $b_{\ell s}$ the corresponding boson operators, the exciton Hamiltonian is defined as (with the convention $\hbar = 1$)

$$\begin{aligned}
 H = & \sum_{\ell s} \omega_0 b_{\ell s}^\dagger b_{\ell s} - A b_{\ell s}^\dagger b_{\ell s}^\dagger b_{\ell s} b_{\ell s} \\
 & + \sum_{\ell=1}^N \Phi (b_{00}^\dagger b_{\ell 1} + b_{\ell 1}^\dagger b_{00}) \\
 & + \sum_{\ell=1}^N \sum_{s=1}^{\infty} \Phi (b_{\ell s}^\dagger b_{\ell s+1} + b_{\ell s+1}^\dagger b_{\ell s}), \quad (1)
 \end{aligned}$$

where ω_0 is the internal frequency of each oscillator, i.e. the energy of an exciton located on a given site, A stands

for the attractive interaction between two excitons that occupy the same site and Φ is the exciton hopping constant between the linked nodes of the network.

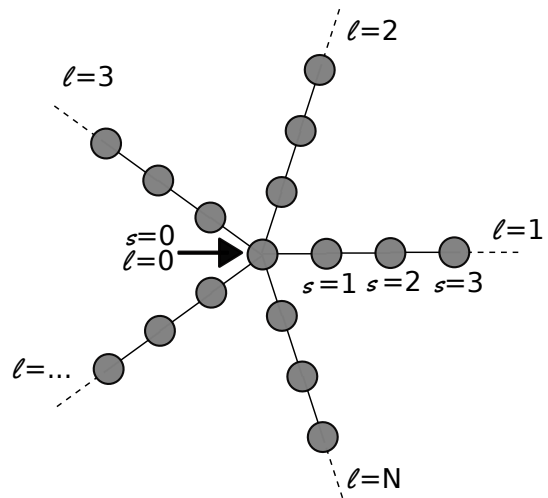


FIG. 1: The extended star graph.

To describe the exciton dynamics, the number state method is applied since the Hamiltonian H conserves the exciton number⁴⁹. Within this method, the Hilbert space E is partitioned into independent subspaces as $E = E_0 \oplus E_1 \oplus E_2 \oplus \dots$, where E_v refers to the v -exciton subspace. The Hamiltonian is thus block-diagonal, each block corresponding to a particular exciton number.

In this work, our aim is to characterize the dynamics that results from the initial creation of two excitons on the core of the star. Therefore, we focus our attention on the E_2 subspace that can be entirely generated by using the local basis $\{|\ell s, \ell' s'\rangle\}$. A particular vector $|\ell s, \ell' s'\rangle$ characterizes two excitons located onto the sites (ℓ, s) and (ℓ', s') , as

$$|\ell s, \ell' s'\rangle = \begin{cases} b_{\ell s}^\dagger b_{\ell' s'}^\dagger |\emptyset\rangle & \text{if } (\ell, s) \neq (\ell', s') \\ \frac{1}{\sqrt{2}} b_{\ell s}^{\dagger 2} |\emptyset\rangle & \text{if } (\ell, s) = (\ell', s'), \end{cases} \quad (2)$$

where $|\emptyset\rangle$ stands for the vacuum state. Note that the basis is normalized and symmetrized to avoid counting twice the same configuration.

B. Schrodinger Equation

In the local basis the two-exciton Schrodinger equation is written as

$$\sum_{\ell_1 s_1} \sum_{\ell'_1 s'_1} (\ell s, \ell' s' | H | \ell_1 s_1, \ell'_1 s'_1) \Psi_{\ell_1 s_1 \ell'_1 s'_1} = \omega \Psi_{\ell s \ell' s'}. \quad (3)$$

As discussed in detail in previous works^{50,55,61}, the calculation of the Hamiltonian matrix elements

$(\ell s, \ell' s' | H | \ell_1 s_1, \ell'_1 s'_1)$ reveals that the Schrodinger equation for the two-exciton wave function $\Psi_{\ell s \ell' s'}$ is isomorphic to a tight-binding model for a single fictitious particle. This particle moves quantum mechanically on a more complex network whose nodes are labeled by the indexes $(\ell s, \ell' s')$. The architecture of that network is schematized in Fig. 2. To be clear, when the fictitious

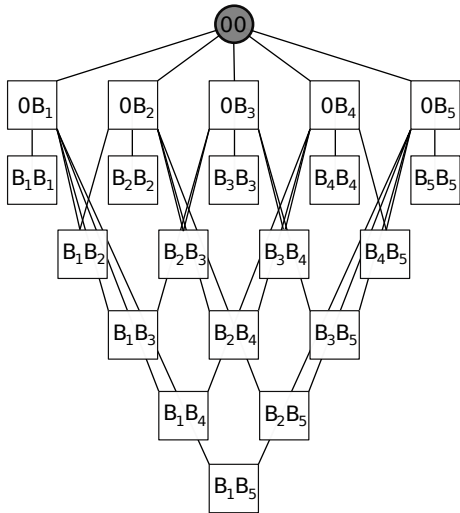


FIG. 2: Schematic view for $N = 5$ of the complex network for the equivalence between the two-exciton dynamics and the tight-binding model for a single fictitious particle (see the text).

particle occupies the top site, this means that the two excitons are located on the core of the star. In other words, the top site for the fictitious particle corresponds to the physical state $|00, 00\rangle$. Then, from a schematic point of view, this site is linked to a set of blocks denoted $(0B_\ell)$ that refer to a situation in which the first exciton is located on the core whereas the second exciton belongs to the branch B_ℓ . Finally, these blocks are linked to many other blocks that correspond to the various ways for distributing the excitons, i.e. either when the two excitons belong to the same branch (blocks $(B_\ell B_\ell)$) or when they belong to distinct branches (blocks $(B_\ell B_{\ell'})$ with $\ell \neq \ell'$).

Within this representation, the Hamiltonian can be easily diagonalized numerically. The knowledge of the corresponding eigenvalues and eigenvectors allows us to solve the Schrodinger equation and to compute the various observables required for describing the dynamics. However, in the strong coupling limit ($A \gg \Phi$), it turns out that the dynamics is mainly governed by pair states involving two excitons "glued" to each other. Restricting our attention to those states, one obtains a simplified problem which provides a simple view of the dynamics, as illustrated in the next sections.

C. The strong coupling limit

In the strong coupling limit ($A \gg \Phi$), states involving two excitons on the same site, whose energy is equal to $2\omega_0 - 2A$, decouple from states in which two excitons lie far from each other and whose energy is equal to $2\omega_0$. Therefore, when the two excitons are initially created on the core of the star, the quantum dynamics is mainly confined in a restriction of the subspace of E_2 , as shown in great details in Refs^{54,55}. According to Fig. 2, this restriction can be built by neglecting the influence of the states describing two exciton belonging to different branches. Therefore, disregarding the blocks $(B_\ell B_{\ell'})$ with $\ell \neq \ell'$, one obtains a first network for the equivalence between the two-exciton dynamics and the tight-binding model for a single fictitious particle, as shown in Fig. 3a.

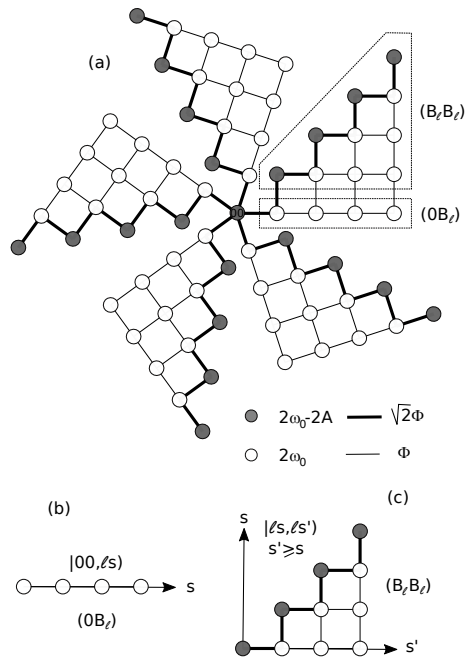


FIG. 3: (a) Complex network for the equivalence between the two-exciton dynamics and the tight-binding model for a single fictitious particle in the strong coupling limit. (b) Tight-binding model in a block $(0B_\ell)$. (c) Tight-binding model in a block $(B_\ell B_\ell)$ (see the text).

This network is a star graph in which the central node refers to the pair state $|00, 00\rangle$. Then, this pair state is connected to the states $|00, \ell s = 1\rangle$ that define the side of the blocks $(0B_\ell)$. As illustrated in Fig. 3b, the block $(0B_\ell)$ refers to the states $|00, \ell s\rangle$ in which an exciton occupies the central node whereas the second exciton is allowed to delocalize along the ℓ th branch. It corresponds to a tight-binding model on a semi-infinite chain. Finally, the states of the block $(0B_\ell)$ are coupled with those of the block $(B_\ell B_\ell)$ which contains all the states $|\ell s, \ell s'\rangle$ with $s' \geq s$. As shown in Fig. 3c, the block $(B_\ell B_\ell)$, that refers to configurations in which the two excitons

occupy the same branch, yields a tight-binding model for the fictitious particle on a 2D lattice which exhibits a row of defects. Note that grey sites describe pair states with self-energy $2\omega_0 - 2A$ whereas white sites, associated to the energy $2\omega_0$, refer to states formed by two excitons located on different sites. The strength of the link is either Φ or $\sqrt{2}\Phi$, depending on the nature of the states involved in the coupling.

In practice, when the two excitons are initially created on the core of the extended star, the relevant states that play the principal role are the pair states. Restricting our attention to the dynamics of those states, the network Fig. 3a can still be simplified by applying standard perturbation theory. To illustrate how perturbation theory works, let us consider two nearest neighbor pair states $|\ell s, \ell s\rangle$ and $|\ell s + 1, \ell s + 1\rangle$ in a given block $(B_\ell B_\ell)$. These two states, whose energy reduces to $2\omega_0 - 2A$, do not interact directly. However, they are coupled with a common state $|\ell s, \ell s + 1\rangle$ whose energy is $2\omega_0$. Due to this coupling, whose strength is equal to $\sqrt{2}\Phi$, the energy of each pair state is renormalized by an amount $-J$ with $J = \Phi^2/A$. In addition, an effective interaction arises between the two pair states whose intensity is $-J$.

By applying the perturbative approach to the network drawn in Fig. 3a, the dynamics of the pair states is described by an effective tight-binding Hamiltonian whose graphical representation corresponds to the network shown in Fig. 4. The architecture of this network is identical to that of the physical extended star graph Fig. 1, but the meaning of both the nodes and the links are rather different. A node labeled by the indexes (ℓ, s) now refers to the pair state $|\ell s, \ell s\rangle$ involving two excitons located on the same site (ℓ, s) of the physical star graph. The central node corresponds to a defect site whose self-energy $2\omega_0 - 2A - N\Phi^2/A$ is red-shifted by an amount $\Delta = (N - 2)\Phi^2/A$ from the self-energy $\epsilon_0 = 2\omega_0 - 2A - 2\Phi^2/A$ of the branch nodes. This defect arises because the pair state $|00, 00\rangle$ is coupled with N branch states $|00, \ell 1\rangle$, $\ell = 1, \dots, N$. By contrast, in a given branch, a pair state $|\ell s, \ell s\rangle$ interact with two states only, i.e. $|\ell s - 1, \ell s\rangle$ and $|\ell s, \ell s + 1\rangle$. Finally, the links between nearest neighbor nodes define the effective pair hopping constant equal to $-J$.

D. Effective Pair state Hamiltonian

According to Fig. 4, the pair dynamics is governed by the following Effective Hamiltonian

$$\begin{aligned} \mathcal{H} = & (\epsilon_0 - \Delta)|0, 0\rangle\langle 0, 0| + \sum_{\ell=1}^N \sum_{s=1}^{\infty} \epsilon_0 |\ell, s\rangle\langle \ell, s| \\ & - \sum_{\ell=1}^N J(|0, 0\rangle\langle \ell, 1| + |\ell, 1\rangle\langle 0, 0|) \\ & - \sum_{\ell=1}^N \sum_{s=1}^{\infty} J(|\ell, s\rangle\langle \ell, s+1| + |\ell, s+1\rangle\langle \ell, s|) \quad (4) \end{aligned}$$

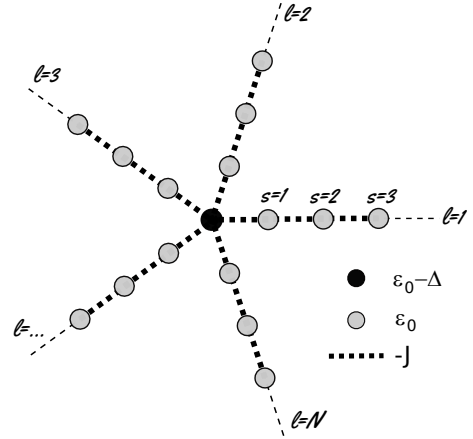


FIG. 4: Effective Hamiltonian that governs the pair states dynamics in the strong A limit (see the text).

where the notation $|\ell, s\rangle \equiv |\ell s, \ell s\rangle$ has been used.

The Hamiltonian \mathcal{H} is invariant under the discrete rotation of angle $\theta = 2\pi/N$ and centered on the central node. Consequently, its diagonalization is simplified when one works with an intermediate basis that involves the pair state localized on the core $|0, 0\rangle$ and a set of orthogonal Bloch states $\{|\chi_s^{(k)}\rangle\}$ with $s \geq 1$ and $k = 1, \dots, N$, defined as

$$|\chi_s^{(k)}\rangle = \frac{1}{\sqrt{N}} \sum_{\ell=1}^N |\ell, s\rangle e^{-ik\ell\theta} \quad (5)$$

Within this basis, k is a good quantum number so that \mathcal{H} becomes block diagonal. It is expressed as a direct sum $\mathcal{H} = \mathcal{H}^{(1)} \oplus \mathcal{H}^{(2)} \dots \oplus \mathcal{H}^{(N)}$ where $\mathcal{H}^{(k)}$ is the block Hamiltonian associated to the quantum number k . Therefore, two situations arise depending on the value of the integer k . For all $k \neq N$, all the block $\mathcal{H}^{(k)}$ are identical. They are expressed as

$$\begin{aligned} \mathcal{H}^{(k \neq N)} = & \sum_{s=1}^{\infty} \epsilon_0 |\chi_s^{(k)}\rangle\langle \chi_s^{(k)}| \\ & - \sum_{s=1}^{\infty} J(|\chi_s^{(k)}\rangle\langle \chi_{s+1}^{(k)}| + |\chi_{s+1}^{(k)}\rangle\langle \chi_s^{(k)}|) \quad (6) \end{aligned}$$

The Hamiltonians $\mathcal{H}^{(k \neq N)}$ is the tight-binding Hamiltonian of a single fictitious particle moving a semi-infinite 1D chain. It involves the Bloch states $|\chi_s^{(k)}\rangle$ with $s \geq 1$ but it does not involve the pair state $|0, 0\rangle$ localized on the core.

For $k = N$, a different situation occurs and the Hamiltonian $\mathcal{H}^{(N)}$ is defined as

$$\begin{aligned} \mathcal{H}^{(N)} = & (\epsilon_0 - \Delta)|0, 0\rangle\langle 0, 0| + \sum_{s=1}^{\infty} \epsilon_0 |\chi_s^{(N)}\rangle\langle \chi_s^{(N)}| \\ & - \sqrt{N} J(|0, 0\rangle\langle \chi_1^{(N)}| + |\chi_1^{(N)}\rangle\langle 0, 0|) \\ & - \sum_{s=1}^{\infty} J(|\chi_s^{(N)}\rangle\langle \chi_{s+1}^{(N)}| + |\chi_{s+1}^{(N)}\rangle\langle \chi_s^{(N)}|) \quad (7) \end{aligned}$$

According to Eq.(7), the pair dynamics is isomorphic to that of a single fictitious particle moving of a semi-infinite chain. This chain involves the sites $s = 0, 1, 2, \dots$ associated to the states $|0, 0\rangle$ (a pair located on the core of the extended star graph), $|\chi_1^{(N)}\rangle$ (a pair uniformly delocalized over the first site $s = 1$ of the branches of the extended star), $|\chi_2^{(N)}\rangle$ (a pair uniformly delocalized over the second site $s = 2$ of the branches of the extended star), ... and so on. When compared with what happens when $k \neq N$, the equivalent lattice exhibits two defects. First, a defect is localized on $s = 0$ whose self-energy is red-shifted when compared with that of the other sites. Second, the strength of the link between the side site $s = 0$ and the site $s = 1$ is equal to $\sqrt{N}J$ whereas in the core of the chain this strength reduces to J .

Within this block diagonal representation of the effective pair state Hamiltonian \mathcal{H} , the corresponding Schrödinger equation can be solved numerically to determine the eigenvalues $\{\omega_\mu^{(k)}\}$ and the associated eigenvectors $\{|\varphi_\mu^{(k)}\rangle\}$ labeled by the indexes k and μ . From the knowledge of these eigen-properties, one can compute in principle all the observables needed for characterizing the dynamics, as illustrated in the next section.

III. NUMERICAL RESULTS

In this section, the previous formalism is applied by considering the initial creation of two excitons on the core of the star. The initial quantum state is thus defined as $|\Psi(0)\rangle = |0, 0\rangle$. Therefore, within the strong coupling limit, the exciton dynamics is governed by the Hamiltonian $\mathcal{H}^{(N)}$ only. The numerical diagonalization of $\mathcal{H}^{(N)}$ yields the eigenvalues $\{\omega_\mu\}$ and the eigenvectors $\{|\varphi_\mu\rangle\}$ whose knowledge allows us to build easily the quantum state $|\Psi(t)\rangle$ at time t . Note that the index N has been removed to simplify the notations.

To characterize the dynamics, several observables can be considered. In this work, we focus our attention on the probability $\pi_s(t)$ to observe the pair at time t in the state $|0, 0\rangle$ (for $s = 0$) or $|\chi_s^{(N)}\rangle$ for $s \geq 1$. This probability provides information about the way the pair either propagates or localizes along the star. Note that in practice, s does not varies from zero to infinity. Instead, a maximum s value is introduced to solve the problem numerically. Therefore, $\pi_s(t)$ does not converge to a stationary value because a unitary dynamics arises. Instead, it fluctuates around a long-time average distribution called the limiting probability $\bar{\pi}_s$ defined as

$$\bar{\pi}_s = \frac{1}{T} \int_0^T \pi_s(t) dt \quad (8)$$

In the following of the text, a special attention will be paid on the influence of the branch number N on the pair properties. The situation $N = 1$, for which the star reduces to a semi-infinite chain, will be disregarded. Note that Φ will be used as energy unit.

A. Space and time dynamics

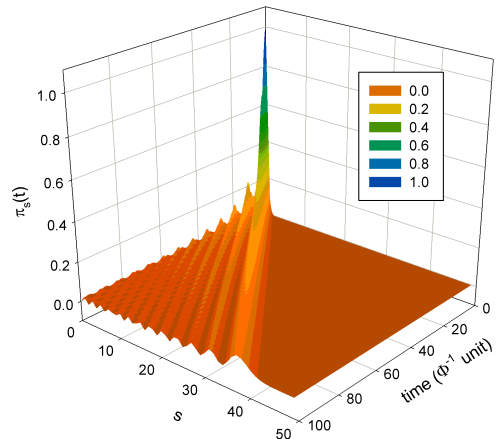


FIG. 5: Space and time evolution of the probability $\pi_s(t)$ for $N = 2$ and $A/\Phi = 5$.

The space and time evolution of the probability $\pi_s(t)$ is shown in Fig. 5 for $N = 2$ and $A/\Phi = 5$. Initially equal to unity, the population of the excited site, i.e. the so-called survival probability to observe the pair where it has been created, decreases slowly. It exhibits damped oscillations whose mean period is approximately equal to $7.8\Phi^{-1}$. Note that its first zero is reached for $t = 6\Phi^{-1}$. This decay of the survival probability is accompanied by the emission of a wave packet. This wave packet propagates rather slowly along the network and it reaches the site $s = 37$ at time $t = 100\Phi^{-1}$. The corresponding velocity is thus approximately equal to $v = 0.37\Phi$.

As shown in Fig. 6 for $A/\Phi = 5$, a fully different behavior takes place when $N = 3$. Indeed, in the short time limit, the population of the excited site rapidly decreases. Nevertheless, in a marked contrast with what happens for $N = 2$, this decay is stopped so that $\pi_0(t)$ does not tend to vanish. Instead, it exhibits damped oscillations around a finite value approximately equal to 0.25. In other words, 25% of the initial energy remains stored in the core of the extended star. The remaining part of the population propagates according as a wave packet. The key point is that the velocity of this wave packet is approximately equal to $v = 0.38\Phi$, similarly to what was observed for $N = 2$.

We have verified that the quantum self-trapping phenomenon observed for $N = 3$ is enhanced as N increases. To illustrate this feature, Fig. 7 shows the space and time evolution of the probability $\pi_s(t)$ for $N = 10$ and $A/\Phi = 5$. In that case, the survival probability rapidly converges towards 0.8, although it still shows damped oscillations. In other words, 80% of the initial energy is now trapped on the core of the star. As previously, this quantum self-trapping is accompanied by the emission of

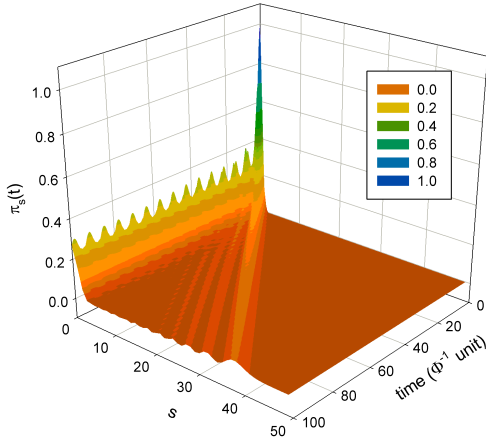


FIG. 6: Space and time evolution of the probability $\pi_s(t)$ for $N = 3$ and $A/\Phi = 5$.

a wave packet that carries the remaining part of the energy. Note that the velocity of the wave packet is still approximately equal to $v = 0.38\Phi$.

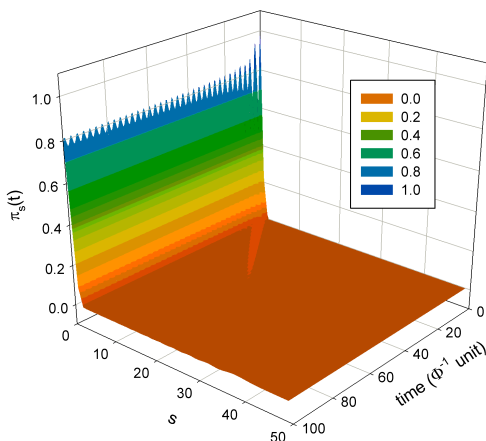


FIG. 7: Space and time evolution of the probability $\pi_s(t)$ for $N = 10$ and $A/\Phi = 5$.

B. Survival probability

The time evolution of the survival probability $\pi_0(t)$ is shown in Fig. 8 for $A/\Phi = 8$ and for different N values. For $N = 2$, as observed in Fig. 5 for $A/\Phi = 5$, the survival probability exhibits damped oscillations. It slowly decreases to reach a very small value which tends to zero as the size of the branches of the star tends to infinity. The mean period of the damped oscillations is approximately equal to $12.5\Phi^{-1}$ and the first zero is reached

for $t = 9.6\Phi^{-1}$. Note that when one compares these results with those displayed in Fig 5, it turns out that these times scale linearly with the coupling strength A . As N becomes larger than 2, a quantum self-trapping takes place. The survival probability no longer vanishes in the long time limit. Instead, it converges towards a finite limiting value $\bar{\pi}_0$ by exhibiting damped oscillations. Both the period and the amplitude of these oscillations decrease as N increases. By contrast, the limiting value increases with N .

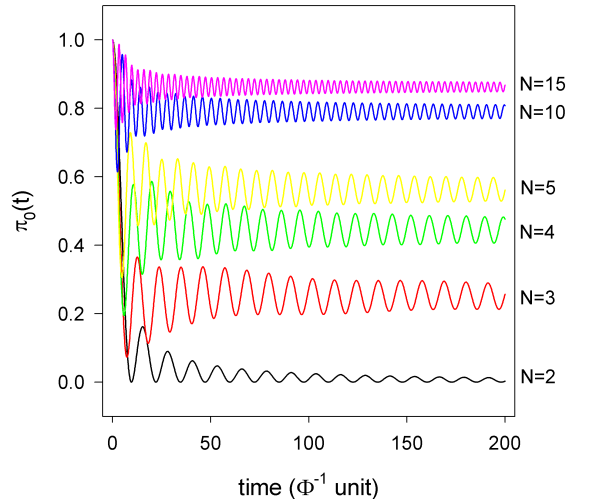


FIG. 8: Time evolution of the survival probability $\pi_0(t)$ for $A/\Phi = 8$ and for different N values.

To clarify this point, the N dependence of the limiting probability is shown in Fig. 9. By considering different A values, we have observed a fundamental property, namely, the limiting probability does not depend on the coupling strength A . It only depends on the branch number N . For $N = 3$, $\bar{\pi}_0 = 0.25$ as observed in Fig. 6 indicating that 25% of the initial population remains self-trapped on the core of the star. For $N = 4$, one obtains a self-trapping of the initial population approximately equal to 44%. The self-trapped population on the core site increases with N . It reaches approximately 80% when N becomes larger than 10, and 90% when N becomes larger than 20.

C. Energy spectrum

To understand these features, let us focus our attention on the nature of the two-exciton eigenstates. The N dependence of the two-exciton eigenenergies in the $k = N$ subspace is displayed in Fig. 10a for $A/\Phi = 5$. When $N = 2$, the energy spectrum exhibits a continuous band centered on ϵ_0 . This band extends from $\epsilon_0 - 0.4\Phi$ to $\epsilon_0 + 0.4\Phi$ so that the resulting bandwidth is equal to 0.8Φ . Note that with $A/\Phi = 5$, this bandwidth corresponds to

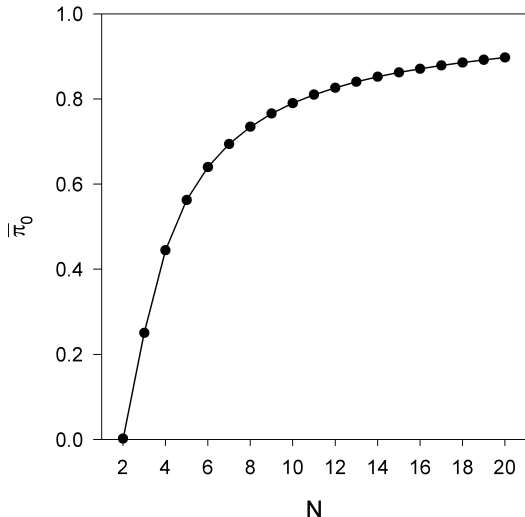


FIG. 9: N dependence of the limiting probability $\bar{\pi}_0$ for $A/\Phi = 8$.

the value $4J$, as expected from the properties of the semi-infinite chain. As N increases, the spectrum still exhibits the continuous band. Nevertheless, it now supports an additional state whose energy is located below the band. The energy of this state decreases as N increases. Equal to $\epsilon_0 - 0.5\Phi$ for $N = 3$, it reaches $\epsilon_0 - 1.82\Phi$ for $N = 10$. Note that the decay of this energy scales linearly with N .

The isolated low energy state defines a localized state whose square modulus of the wave function is displayed in Fig. 10b for various N values. It describes a pair whose wave function localizes on the core of the extended star and whose amplitude decreases as one moves away from the core along the branches. The strength of the localization is enhanced as N increases. To illustrate this feature, we have studied the behavior of the localization length ξ assuming that the low energy state wave function scales as $\exp(-s/\xi)$ for large s values. It results that ξ decreases as N increases. It is successively equal to 0.72, 0.45 and 0.38 for $N = 5, 10$ and 15, respectively.

IV. DISCUSSION AND CONCLUSION

In the previous sections, we have shown that in the strong coupling limit and when the two excitons are created on the core of the extended star, the quantum dynamics is dominated by pair states. In such states, the two excitons are "glued" to each other. They thus behave as a single particle whose dynamics is described by a tight-binding model on a semi-infinite chain. Along that chain, the site $s = 0$ refers to a pair located on the core of the extended star whereas the sites $s \geq 1$ describe a pair uniformly delocalized over the s th sites of the branches of the star.

In that context, our numerical results reveal the oc-

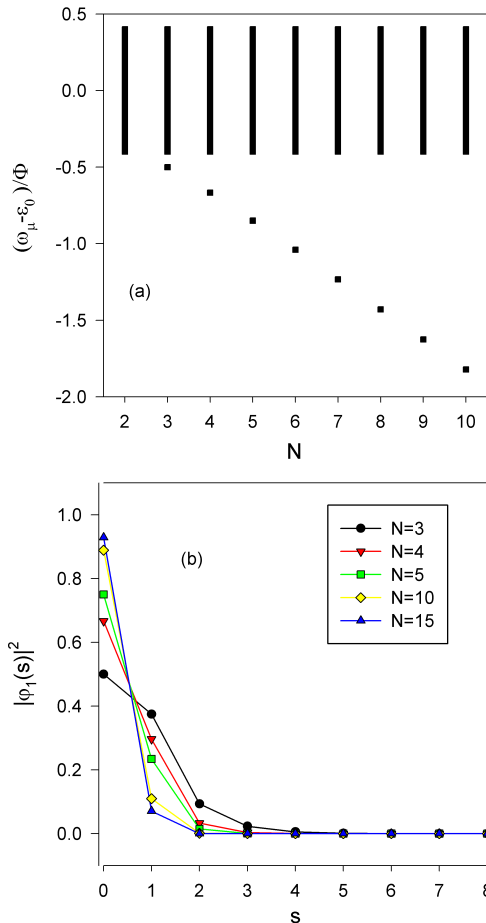


FIG. 10: (a) N dependence of the two-exciton eigenenergies in the $k = N$ subspace for $A/\Phi = 5$. (b) Square modulus of the low energy state wave function.

currence of a real quantum self-trapping whose properties mainly depend on the architecture of the extended star. More precisely, when the branch number reduces to $N = 2$, the energy does not self-localize. Instead, it propagates along the branches according to a wave packet that spreads out as it moves. This result is not surprising since for $N = 2$, the extended star corresponds to an infinite chain with translational invariance. In that case, TEBS cannot localize the energy because they must share the symmetry of the translation operator. They thus correspond to Bloch waves that belong to a finite width energy band.

In a marked contrast, when $N \geq 3$, a fully different behavior arises. The two excitons experience a real quantum self-trapping so that they tend to localize on the core of the star. Quite surprisingly, the strength of the self-localization does not depend on the coupling parameter A . Instead, it is governed by the branch number so that it is enhanced as N increases. In fact, we have shown that the quantum self-trapping originates in the restructuring of the pair eigenstates. As N increases, a

low-energy state occurs below a continuous band. This state describes a pair whose wave function localizes exponentially on the core of the star. As a result, the initial creation of two excitons on the core excites preferentially this localized state. Therefore, the main part of the energy stays trapped where it has been deposited. Nevertheless, the initial quantum state also involves propagating states that belong to the continuous band, but to a lesser extent. Consequently, a small part of the initial energy is carried by those states according as a wave packet which emanates out from the central core and propagates along the branches.

To interpret these observed features, let us characterize the relevant pair states, i.e. the eigenstates of the Hamiltonian $\mathcal{H}^{(N)}$ Eq.(7). As described previously, these pair states are isomorphic to those of a single particle moving on the semi-infinite chain shown in Fig. 11. The

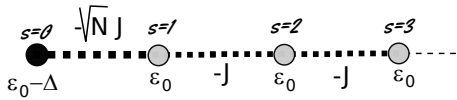


FIG. 11: Effective tight-binding Hamiltonian that governs the relevant pair states dynamics in the strong coupling limit. $s = 0$ refers to a pair located on the core of the star whereas $s \geq 1$ describe a pair uniformly delocalized over the s th sites of the branches.

corresponding Schrodinger equation is expressed as

$$\begin{aligned} -\sqrt{N}J\varphi(1) + (\epsilon_0 - \Delta)\varphi(0) &= \omega\varphi(0) \\ -\sqrt{N}J\varphi(0) + \epsilon_0\varphi(1) - J\varphi(2) &= \omega\varphi(1) \\ &\dots = \dots \\ -J\varphi(s-1) + \epsilon_0\varphi(s) - J\varphi(s+1) &= \omega\varphi(s) \\ &\dots = \dots \end{aligned} \quad (9)$$

where $\varphi(s)$ is the pair wave function with energy ω .

According to the standard properties of the tight-binding model^{62,63}, it is straightforward to show that the semi-infinite chain supports extended states. Indeed, far from the side site $s = 0$, the Schrodinger equation Eq.(9) reduces to that of a linear chain with translational invariance. Therefore, when one considers the presence of the boundary $s = 0$, it turns out that the Hamiltonian $\mathcal{H}^{(N)}$ exhibits eigenstates that correspond to superpositions of forward and backward traveling waves as

$$\varphi_q(s) = \beta_q^{(+)} e^{iqs} + \beta_q^{(-)} e^{-iqs}. \quad (10)$$

These waves, characterized by a real wave vector q , define a continuous band $\omega \in [\epsilon_0 - 2J, \epsilon_0 + 2J]$ that contains the eigenenergies $\omega_q = \epsilon_0 - 2J \cos(q)$. They describe pair states uniformly delocalized over the branches of the star and that propagate along that branches.

However, since the semi-infinite chain Fig. 11 exhibits defects which break the symmetry of the problem, the Hamiltonian $\mathcal{H}^{(N)}$ supports an additional state whose properties strongly differ from those of the traveling waves. To illustrate this feature, let us seek a solution

of Eq.(9) as⁶²

$$\varphi(s) = \begin{cases} \alpha & \text{if } s = 0 \\ \beta e^{iqs} & \text{if } s \geq 1. \end{cases} \quad (11)$$

By inserting this solution in Eq.(9) for $s > 1$, it turns out that the corresponding eigenenergy still satisfies the dispersion relation of the infinite chain $\omega = \epsilon_0 - 2J \cos(q)$. Then, by inserting Eq.(11) in Eq.(9) for $s = 0$ and $s = 1$, one obtains a relation between α and β , namely $\beta = \sqrt{N}\alpha$. Moreover, the value of the wave vector q , still unknown at this stage, is given by the following equation

$$(1 - N)e^{iq} + e^{-iq} = \frac{\Delta}{J}. \quad (12)$$

Since $\Delta/J = (N - 2)$, this equation exhibits a complex solution $q = i/\xi$ provided that $N \geq 2$. The so-called localization length ξ is defines as

$$\xi = \frac{1}{\ln(N - 1)}. \quad (13)$$

The resulting wave function is thus expressed as

$$\varphi_L(s) = \sqrt{\frac{N-2}{N-1}} \left[\delta_{s0} + (1 - \delta_{s0})\sqrt{N}e^{-s/\xi} \right], \quad (14)$$

and the corresponding eigenenergy is written as

$$\omega_L = \epsilon_0 - 2J - J \frac{(N-2)^2}{N-1}. \quad (15)$$

In a perfect agreement with the results displayed in Fig. 10, the solution Eq.(14) defines a localized state provided that $N > 2$. It characterizes a pair whose wave function decreases exponentially as one moves away from the core of the extended star. The energy of the localized state is located below the continuous band. It is red-shifted from the low-energy band edge $\epsilon_0 - 2J$ by an amount $\delta\omega = J(N-2)^2/(N-1)$. Note that the case $N = 2$ describes an extended state whose localization length diverges ($\xi \rightarrow \infty$) and whose energy is equal to the band edge $\delta\omega = 0$. A remarkable feature is that most of the properties of the localized state only depends on the branch number. This is the case for the localization length Eq.(13) that exhibits a logarithmic divergence when with respect to N . This is also the case for the wave function Eq.(14) whose localized nature is enhanced as N increases. Only the energy involves the nonlinearity A through its dependence with respect to the effective pair hopping constant $J = \Phi^2/A$.

The initial creation of two excitons on the core of the star brings the pair in a superposition that involves both the localized state and the traveling waves. According to Eq.(14), the weight of the localized state equal to $(N-2)/(N-1)$ increases as N increases. By contrast, the weight of the traveling waves, that reduces to $1/(N-1)$, decays with the branch number. As time elapses, the pair quantum state behaves as

$$\Psi_s(t) = e^{-i\omega_L t} \varphi_L(s) \varphi_L^*(0) + \sum_q e^{-i\omega_q t} \varphi_q(s) \varphi_q^*(0). \quad (16)$$

Two situation arises. For $N = 2$, $\varphi_L(s) = 0$ so that $\Psi_s(t)$ reduces to a traveling wave. In that case, the extended star corresponds to an infinite chain with translational invariance so that there is no self-trapping. The pair behaves as a single particle that delocalizes along the chain, the corresponding propagator being given by a Bessel function of the first kind as $\Psi_s(t) \propto J_s(2Jt)^{54}$. By contrast, when $N \geq 3$, the first term in the right end side of Eq.(16) shows that the main part of the energy remains trapped in the localized state. It self-localizes in an exponential way in the neighborhood of the central core of the star graph. The second term in the right end side of Eq.(16) indicates that the remaining part of the deposited energy is carried by the traveling waves. These waves are responsible for the emission of a wave packet that propagates along the branches of the extended star. In the long time limit, i.e. when the wave packet has left the excited region, the quantum probabilities $\pi_s(t) = |\Psi_s(t)|^2$ converge towards their limiting values $\bar{\pi}_s = |\varphi_L(s)\varphi_L^*(0)|^2$ expressed as

$$\bar{\pi}_s = \left(\frac{N-2}{N-1}\right)^2 \left[\delta_{s0} + (1 - \delta_{s0})N e^{-2s/\xi} \right]. \quad (17)$$

As observed in the numerical section (see Fig. 9), the limiting probabilities only depends on the branch number. The survival probability $\bar{\pi}_0 = (N-2)^2/(N-1)^2$ increases with N . By contrast, $\bar{\pi}_1$ first increases with the branch number until N reaches 4. Then, it decreases as N increases. Finally, for $s \geq 2$, $\bar{\pi}_s$ is a decaying function of the branch number provided that $N \geq 3$.

These results clearly show that in the strong coupling limit, the branch number is the key parameter that controls the strength of the quantum self-trapping. As N increases, an important restructuring of the pair eigenstates arises. The localized nature of the low-energy state is strongly enhanced so that the self-localization of the deposited energy intensifies.

V. CONCLUSION

In the present paper, the Bose-Hubbard model has been used to analyze the quantum self-trapping in an

extended star graph. Within this model, we have shown that in the strong coupling limit and when two excitons are created on the core of the star, the dynamics is dominated by pair states, that is “glued” excitons behaving as a single particle. It turns out that the degree N of the core site governs the pair properties so that two situations arises. When $N = 2$, the star reduces to a linear chain so that the energy does not self-localize. Instead, it propagates along the branches of the star according as a wave packet that spreads out as it moves. Conversely, when $N \geq 3$, an important restructuring of the pair eigenstates arises and a low-energy localized state occurs. This state describes a pair whose wave function localizes exponentially on the core of the extended star. The initial creation of two excitons on the core excites preferentially this localized state so that the main part of the energy self-localizes where it has been deposited. Nevertheless, a small part of the initial energy is carried by the remaining traveling waves according as a wave packet which emanates out from the central core and propagates along the branches. As N increases, this process is enhanced and a stronger quantum self-trapping takes place.

This work is based on the assumption of a strong exciton-exciton coupling. Consequently, the coupling strength does not play a significant role in the occurrence of a self-trapping, apart from allowing the creation of pair states. In forthcoming works, it would be wise to go beyond this approximation in order to investigate the role of the coupling on the ability to self-localize the energy. Moreover, it would be interesting to analyze the influence of the initial conditions, i.e. to create either a pair outside the core of the star or two excitons lying far apart. The self-trapping could compete with degeneracy-induced localization that arises in complex networks.

* Electronic address: vincent.pouthier@univ-fcomte.fr

¹ O. Mulken and A. Blumen, *Phys. Rep.* **502**, 37 (2011).

² D. Astruc, E. Boisselier, and C. Ornelas, *Chem. Rev.* **110**, 1857 (2010).

³ S. Tretiak, V. Chernyak, and S. Mukamel, *J. Phys. Chem. B* **102**, 3310 (1998).

⁴ E. Y. Poliakov, V. Chernyak, S. Tretiak, and S. Mukamel, *J. Chem. Phys.* **110**, 8161 (1999).

⁵ K. Harigaya, *Chem. Phys. Lett.* **300**, 33 (1999).

⁶ G. W. Crabtree and N. S. Lewis, *Phys. Today* **60**, 37 (2007).

⁷ C. Supritz, V. Gounaris, and P. Reineker, *J. Lumin.* **128**, 877 (2008).

⁸ M. Nakano, R. Kishi, T. Minami, and K. Yoneeda, *Molecules* **14**, 3700 (2009).

⁹ V. M. Freixas, D. Ondarse-Alvarez, S. Tretiak, D. V. Makhov, D. V. Shalashilin, and S. Fernandez-Alberti, *J. Chem. Phys.* **150**, 124301 (2019).

¹⁰ A. Bar-Haim, J. Klafter, and R. Kopelman, *J. Am. Chem. Soc.* **119**, 6197 (1997).

¹¹ M.S. Choi, T. Aida, T. Yamazaki, and I. Yamazaki, *Chem. Eur. J.* **8**, 2667 (2002).

- ¹² O. Mulken, V. Bierbaun, and A. Blumen, *J. Chem. Phys.* **124**, 124905 (2006).
- ¹³ A. M. Childs, *Phys. Rev. Lett.* **102**, 180501 (2009).
- ¹⁴ E. Farhi, J. Goldstone, and S. Gutmann, *Theory Comput.* **4**, 169 (2008).
- ¹⁵ A. M. Childs, E. Farhi, and S. Gutmann, *Quant. Info. Proc.* **1**, 35 (2002).
- ¹⁶ E. Farhi and S. Gutmann, *Phys. Rev. A* **57**, 2403 (1998).
- ¹⁷ A. M. Childs and J. Goldstone, *Phys. Rev. A* **70**, 022314 (2004).
- ¹⁸ L. K. Grover, *Phys. Rev. Lett.* **79**, 325 (1997).
- ¹⁹ M. Mohseni, P. Rebentrost, S. Lloyd, and A. Aspuru-Guzik, *J. Chem. Phys.* **129**, 174106 (2008).
- ²⁰ S. R. Jackson, T. J. Khoo, and F. W. Strauch, *Phys. Rev. A* **86**, 022335 (2012).
- ²¹ A.L. Cardoso, R.F.S. Andrade, and A.M.C. Souza, *Phys. Rev. B* **78**, 214202 (2008).
- ²² Z. Darazs, A. Anishchenko, T. Kiss, A. Blumen, and O. Mulken, *Phys. Rev. E* **90**, 032113 (2014).
- ²³ E. Agliari, A. Blumen, and O. Mulken, *Phys. Rev. A* **82**, 012305 (2010).
- ²⁴ O. Mulken, M. Dolgushev, and M. Galiceanu, *Phys. Rev. E* **93**, 022304 (2016).
- ²⁵ S. Salimi, *Ann. Phys.* **324**, 1185 (2009).
- ²⁶ A. Ziletti, F. Borgonovi, G.L. Celardo, F.M. Izrailev, L. Kaplan, and V.G. Zelevinsky, *Phys. Rev. B* **85**, 052201 (2012).
- ²⁷ X.P. Xu, *Phys. Rev. E* **79**, 011117 (2009).
- ²⁸ A. Anishchenko, A. Blumen, and O. Mulken, *Quantum Inf. Process* **11**, 1273 (2012).
- ²⁹ V. Pouthier, *Quantum Inf. Process* **14**, 491 (2015).
- ³⁰ V. Pouthier, *Quantum Inf. Process* **14**, 3139 (2015).
- ³¹ S. Yalouz, V. Pouthier, and C. Falvo, *Quantum Inf. Process* **16**, 143 (2017).
- ³² O. Mulken and A. Blumen, *Phys. Rev. E* **73**, 066117 (2006).
- ³³ Y. Yin, D. E. Katsanos, and S. N. Evangelou, *Phys. Rev. A* **77**, 022302 (2008).
- ³⁴ O. Mulken, V. Bierbaum, and A. Blumen, *Phys. Rev. E* **75**, 031121 (2007).
- ³⁵ P. Rebentrost, M. Mohseni, I. Kassal, S. Lloyd, and A. Aspuru-Guzik, *New. J. Phys.* **11**, 033003 (2009).
- ³⁶ J. P. Keating, N. Linden, J. C. F. Matthews, and A. Winter, *Phys. Rev. A* **76**, 012315 (2007).
- ³⁷ S. R. Jackson, T. J. Khoo, and F. W. Strauch, *Phys. Rev. A* **86**, 022335 (2012).
- ³⁸ V. Pouhtier, *J. Chem. Phys.* **139**, 234111 (2013).
- ³⁹ A.C. Scott, *Phys. Rep.* **217**, 1 (1992).
- ⁴⁰ A.J. Sievers and S. Takeno, *Phys. Rev. Lett.* **61**, 970 (1988).
- ⁴¹ S. Flach and C.R. Willis, *Phys. Rep.* **295**, 181 (1998).
- ⁴² J.C. Eilbeck, P.S. Lomdahl, and A.C. Scott, *Physica D* **16**, 318 (1985).
- ⁴³ G. Kalosakas, A.R. Bishop, and V.M. Kenkre, *Phys. Rev. A* **68**, 023602 (2003).
- ⁴⁴ S. Yalouz, B. Senjean, F. Miatto, and V. Dunjko, *Quantum* **5**, 572 (2021).
- ⁴⁵ J.C. Kimball, C.Y. Fong, and Y.R. Shen, *Phys. Rev. B* **23**, 4946 (1981).
- ⁴⁶ F. Bogani, G. Cardini, V. Schettino, and P.L. Tasselli, *Phys. Rev. B* **42**, 2307 (1990).
- ⁴⁷ E. Wright, J.C. Eilbeck, M.H. Hays, P.D. Miller, and A.C. Scott, *Physica D* **69**, 18 (1993).
- ⁴⁸ L. Bernstein, J.C. Eilbeck, and A.C. Scott, *Nonlinearity* **3**, 293 (1990).
- ⁴⁹ A.C. Scott, J.C. Eilbeck, and H. Gilhoj, *Physica D* **78**, 194 (1994).
- ⁵⁰ V. Pouthier, *Phys. Rev. E* **68**, 021909 (2003).
- ⁵¹ V. Pouthier, *J. Chem. Phys.* **118**, 9364 (2003).
- ⁵² J. Doriganc, J.C. Eilbeck, M. Salerno, A.C. Scott, *Phys. Rev. Lett.* **93**, 025504 (2004).
- ⁵³ L. Proville, *Phys. Rev. B* **71**, 1043306 (2005).
- ⁵⁴ C. Falvo, V. Pouthier, and J.C. Eilbeck, *Physica D* **221**, 58 (2006).
- ⁵⁵ V. Pouthier, *Phys. Rev. B* **76**, 224302 (2007).
- ⁵⁶ P. Guyot-Sionnest, *Phys. Rev. Lett.* **67**, 2323 (1991).
- ⁵⁷ P. Jakob, *Phys. Rev. Lett.* **77**, 4229 (1996).
- ⁵⁸ R. Honke, P. Jakob, Y. J. Chabal, A. Dvorak, S. Tausendpfund, W. Stigler, P. Pavone, A. P. Mayer, and U. Schröder, *Phys. Rev. B* **59**, 10996(1999).
- ⁵⁹ P. Jakob, *J. Chem. Phys.* **114**, 3692 (2001).
- ⁶⁰ J. Edler, R. Pfister, V. Pouthier, C. Falvo, and P. Hamm, *Phys. Rev. Lett.* **93**, 106405 (200).
- ⁶¹ V. Pouthier, *Phys. Rev. E* (submitted).
- ⁶² M.C. Desjonqueres and D. Spanjaard, *Concepts in Surface Physics* (Springer-Verlag, Berlin, 1996).
- ⁶³ H. Li, S.V. Malinin, S. Tretiak, and V.Y. Chernyak, *J. Chem. Phys.* **139**, 064109 (2013).